

Drag coefficient reduction at very high wind speeds

John A. T. Bye¹ and Alastair D. Jenkins²

Received 21 June 2005; revised 25 November 2005; accepted 10 December 2005; published 31 March 2006.

[1] The correct representation of the 10-m drag coefficient for momentum (K_{10}) at extreme wind speeds is very important for modeling the development of tropical depressions and may also be relevant to the understanding of other intense marine meteorological phenomena. We present a unified boundary layer model for (K_{10}), which takes account of both the wave field and spray production, and asymptotes to the growing wind wave state in the absence of spray. The theoretical development is based on an air-sea system with shear layers in both fluids and contains three constants that must be determined empirically. This is done using data from observations, and the resulting behavior is interpreted in terms of spray. A feature of the results is the prediction of a broad maximum in K_{10} . For a spray velocity of 9 m s^{-1} , it is found that a maximum of $K_{10} \sim 2.0 \times 10^{-3}$ occurs for a 10-m wind speed, $u_{10} \sim 40 \text{ m s}^{-1}$, in agreement with recent GPS sonde data in tropical cyclones. Thus K_{10} is “capped” at its maximum value for all higher wind speeds expected. A physically based model, where spray droplets are injected horizontally into the airflow and maintained in suspension by air turbulence, gives qualitatively similar results. The effect of spray is also shown to flatten the sea surface by transferring energy to longer wavelengths.

Citation: Bye, J. A. T., and A. D. Jenkins (2006), Drag coefficient reduction at very high wind speeds, *J. Geophys. Res.*, *111*, C03024, doi:10.1029/2005JC003114.

1. Introduction

[2] It is of importance to be able to accurately parameterize air-sea exchange processes at extreme wind speeds in order to understand the mechanisms which control the evolution of tropical cyclones [Emanuel, 2003]. There are also indications that rapid increases in wind speed may tend to depress the height of surface waves and thus perhaps reduce the drag coefficient by the flattening of sea surface roughness elements [Jenkins, 2002]. Here we consider momentum exchange, and present a seamless formulation which predicts the drag coefficient over the complete range of wind speeds. The results are calibrated against the data set of Powell *et al.* [2003], obtained by Global Positioning System dropwindsonde (GPS sonde) releases in tropical cyclones. The theoretical development is based on an air-sea system with shear layer in both fluids, and contains three constants that must be determined empirically. This is performed using the properties of the fully developed growing wind wave sea, and two field data sets collected in storm systems, and the resulting behavior is interpreted in terms of spray.

[3] The basis of the analysis is to apply a general expression for the drag coefficient (K_{10}), that has been derived from the inertial coupling relations [Bye, 1995], which take account of the wave field [Bye *et al.*, 2001], to

the wave boundary layer [Bye, 1988] in the situation occurring under very high wind speeds, when spray plays a significant role in the air-sea momentum transfer. The analysis shows how the production of spray may play an essential role in the frictional regime which prevails in storm systems. The inertial coupling relation may be regarded as a parameterization of the dynamical effect of ocean waves within the coupled system containing the atmospheric and oceanic near-surface turbulent boundary layers [Jenkins, 1989, 1992].

[4] We outline the derivation of the general expression for the 10-m drag coefficient and the Charnock constant [Charnock, 1955] in section 2, and then (section 3) introduce a simple formulation, which characterizes the sea state in storm systems, and gives rise to a maximum in the 10-m drag coefficient. In section 4, the inertially coupled boundary layer analysis is interpreted in terms of spray production, which is thought to be of great importance in very high wind conditions; see, for example, Lighthill [1999]. In particular, in section 4.6, a physical model in which spray droplets are injected horizontally into the airflow and are maintained in suspension by turbulence is introduced, which gives qualitatively similar predictions for the variation of the 10-m drag coefficient with wind speed.

2. General Expressions for the 10-m Drag Coefficient (K_{10}) and the Charnock Constant (α)

[5] In the wave boundary layer [Bye, 1988],

$$u_{10} = u_1 - (u_* / \kappa) \ln(z_B / z_{10}), \quad (1)$$

¹School of Earth Sciences, University of Melbourne, Melbourne, Victoria, Australia.

²Bjerknes Centre for Climate Research, Bergen, Norway.

where u_{10} is the wind velocity at 10 m, $z_{10} = 10$ m, and u_1 (which will be called the surface wind) is the wind velocity at the height $z_B = 1/(2k_0)$, where k_0 is the peak wave number of the wave spectrum, u_* is the friction velocity and $\kappa = 0.4$ is von Kármán's constant. On introducing the inertial coupling relationships [Bye, 1995; Bye and Wolff, 2004],

$$u_* = K_I^{1/2}(u_1 - u_2/\varepsilon) \quad (2)$$

$$\varepsilon u_L = \frac{1}{2}(\varepsilon u_1 + u_2) \quad (3)$$

in which the reference velocity has been set equal to zero for convenience, K_I is the inertial drag coefficient, and $\varepsilon = (\rho_1/\rho_2)^{1/2}$, where ρ_1 and ρ_2 are the densities of air and water, respectively, and u_2 (which will be called the surface current) is the current velocity at the depth z_B , at which the particle velocities in the wave motion become negligible, and εu_L is the wave-induced velocity in water (the spectrally integrated surface Stokes velocity (the surface Stokes drift velocity)), and u_L is the wave-induced velocity in air (the spectrally weighted phase velocity), and also the relation [Bye and Wolff, 2001]

$$\varepsilon u_L = r(-u_2), \quad (4)$$

where r is the ratio of the Stokes shear to the Eulerian shear in the water. We obtain the drag law

$$u_*^2 = K_R u_1^2 \quad (5a)$$

in which

$$K_R = K_I/R^2, \quad (5b)$$

where $R = \frac{1}{2}(1 + 2r)/(1 + r)$, and K_R is the intrinsic drag coefficient for the coupled system. For $R = 1$, in which the Eulerian shear in the water is negligible in comparison with the Stokes shear, $K_R = K_I$. In the situation in which the Eulerian shear opposes the Stokes shear ($r < 0$), a frictional drag occurs in which $R > 1$, and $K_R < K_I$, which indicates the formation of a "slip" surface at the air-sea interface. On now substituting for u_1 in (1), we obtain

$$1/\sqrt{K_{10}} = (1/\sqrt{K_R}) - (1/\kappa) \ln[1/(2z_{10}k_0)], \quad (6)$$

where $K_{10} = u_*^2/u_{10}^2$ is the 10-m drag coefficient. Next, with the introduction of the relation

$$c_0/u_1 = B, \quad (7)$$

where B is the ratio of the phase speed of the peak wave, $c_0 = (g/k_0)^{1/2}$, to the surface wind, u_1 , g being the acceleration due to gravity, equation (6) yields the 10-m drag relation

$$1/\sqrt{K_{10}} = (1/\sqrt{K_R}) - (1/\kappa) \ln[B^2 u_*^2 / (2z_{10} g K_R)] \quad (8)$$

and (5) yields the expression for the wave age,

$$c_0/u_* = B/\sqrt{K_R}. \quad (9)$$

Finally, on defining the Charnock constant,

$$\alpha = z_0 g / u_*^2, \quad (10)$$

where the air-sea roughness length (z_0) satisfies the relation

$$(1/\kappa) \ln(z_{10}/z_0) = 1/\sqrt{K_{10}}, \quad (11)$$

we obtain, from (8), the expression

$$\alpha = \frac{1}{2}(B^2/K_R) \exp(-\kappa/\sqrt{K_R}). \quad (12)$$

Equations (8) and (12) are general expressions for K_{10} and α , respectively, in terms of the wave boundary layer parameters K_R and B .

[6] It is the purpose of this paper to apply these relations to model the form of the 10-m drag coefficient at the very high wind speeds, which occur in hurricanes, where spray may have an important influence. The hurricane is the most intense example of a cyclonic storm system in which the effects of rotation are clearly of importance. At the outset, however, we retreat to the simpler environment characterized by the growing wind wave sea, in which rotation plays a negligible role.

3. Characterization of Sea States by the Frictional Regime, Which Occurs in the Wave Boundary Layer

[7] The inertial coupling formulation introduced in section 2 incorporates the frictional regime of the wave boundary layer through the parameter, r in (4), or equivalently, the parameter R in (5). We consider first the situation for the growing wind wave sea.

3.1. Fully Developed Growing Wind Wave Sea

[8] The wave field in the growing wind wave sea is generated impulsively by an ideal steady rectilinear wind. The fully developed growing wind wave sea occurs when the wave field is independent of fetch. In this situation, it was shown by Bye and Wolff [2001], by evaluating both the spectrally integrated surface Stokes velocity (the Stokes drift) and the spectrally weighted phase velocity of the wave spectrum that the Stokes shear dominates the Eulerian shear, $r \rightarrow \pm\infty$ ($R = 1$), such that the intrinsic drag coefficient (K_R) is the inertial drag coefficient (K_I). The properties of the fully developed growing wind wave sea, in which (1) the Charnock constant $\alpha = 0.018$ [Wu, 1980] and (2) the inverse wave age $u_*/c_0 = A$, where $A = 0.029$ [Toba, 1973], can be used to estimate K_I and B . On substituting the conditions 1 and 2 in (12), with $R = 1$, we obtain $K_I = 1.5 \times 10^{-3}$, and on substituting for K_I in (9) with $R = 1$, $B = 1.3$. We will use these estimates of K_I and B below when considering the wind sea in a storm system. An extended discussion of the application of the

Table 1. Storm System Data Sets

	u_{10} , m s ⁻¹	u_* , m s ⁻¹	K_{10} , 10 ⁻³	R
MBL ^a 30–39	27	1.15	1.81	1.13
MBL ^a 40–49	34	1.55	2.07	1.13
MBL ^a 50–59	40	1.85	2.14	1.15
MBL ^a 60–69	52	2.20	1.78	1.29
JASIN ^b	7.5	0.26	1.20	1.03

^aMBL x - y , mean boundary layer wind speed group (m s⁻¹). Estimates of u_* and K_{10} have been extracted from Figures 3a and 3c, respectively, of Powell *et al.* [2003].

^bJASIN (Joint Air-Sea Interaction) experiment, mean wind speed (m s⁻¹). Estimates of u_* and K_{10} have been extracted from Figure 1 of Nicholls [1985].

inertial coupling relations to the fully developed growing wind wave sea is given by *Bye and Wolff* [2004], in which it is shown that K_I should remain approximately constant in more general wave conditions. The parameter B would be expected to be approximately constant because of the fetch-independent conditions which occur in the storm systems.

3.2. Frictional Balance in a Storm System

[9] In a storm system, rotation plays an important role. The frictional balance can be addressed through a model of the coupled Ekman layers of the ocean and the atmosphere. A suitable model has been developed by *Bye* [2002], in which the velocity and shear stress at the edge of the wave boundary layer in the ocean and the atmosphere are matched with an outer layer of constant density and viscosity using the inertial coupling relation (2). This model is of similar form to the steady state two-layer planetary boundary layer (PBL), which has been found to provide a good representation of the PBL velocity structure over land [*Garratt and Hess*, 2003].

[10] In the model, the eddy viscosities in the constant viscosity layers in the atmosphere and ocean are represented by the similarity expressions:

$$v_1 = C\kappa u_*^2/f; \quad (13a)$$

$$v_2 = C\kappa w_*^2/f, \quad f > 0, \quad (13b)$$

where $w_* = \varepsilon u_*$, and $f = 2\Omega \sin\phi$ is the Coriolis parameter, in which Ω is the angular speed of rotation of the Earth, ϕ is the latitude, C is a similarity constant, and the matching of the two layers in the atmosphere occurs at $z_B = Cu_*/f$. A key result was that

$$r = -\left\{1 + [C\kappa/(2K_I)]^{1/2}\right\}, \quad (14)$$

which demonstrates that, since $C > 0$, a steady state equilibrium is only possible for $-\infty < r < -1$ ($R > 1$) [*Bye*, 2002]. Equation (14) links the frictional properties in the inner wave boundary layer and the outer constant viscosity layer of the Ekman layer, and shows that r is determined by the constant (C).

[11] It was also found that for a zero reference velocity in the ocean, the geostrophic drag coefficient and the angle of rotation of the surface shear stress to the left-hand side (in

the Northern Hemisphere) of the surface geostrophic velocity in the atmosphere (u_g) are

$$K_g = u_*^2/u_g^2 = K_I(r+1)^2/(r^2+1) \quad (15a)$$

$$\mu = \tan^{-1}(-1/r) \quad (15b)$$

respectively. Thus the wave field in the storm system is controlled by a different frictional regime to the fully developed growing wind wave sea. This regime is characterized by an angle of turning (μ), which is determined by the frictional parameter (r).

[12] We will consider two data sets that have been obtained in storm systems, which enable r (or R) to be determined. The first data set was obtained in moderate conditions in the Joint Air-Sea Interaction (JASIN) experiment in the Atlantic Ocean northwest of Scotland [*Nicholls*, 1985]. The second data set was obtained in very high wind speeds in the tropical Atlantic and Pacific Oceans during the passage of 15 hurricanes [*Powell et al.*, 2003]. These data are summarized in Table 1 in four ranges of u_{10} for the hurricane data, and for the mean conditions of the JASIN experiment, and the corresponding values of R have been obtained by the numerical solution of (8), using $g = 9.8 \text{ m s}^{-2}$, $\kappa = 0.4$, $K_I = 1.5 \times 10^{-3}$, and $B = 1.3$.

[13] Figure 1 indicates that the data can be fitted by a linear regression in which

$$1 - (1/R) = au_*, \quad (16)$$

where $a = 0.087 \text{ m}^{-1} \text{ s}$, although there is a considerable scatter, which arises from the sensitivity of R to the mean observed value of u_* for each u_{10} range. The substitution of (5a) in (16) yields

$$R = R_0 + u_1/q_0 \quad (17a)$$

$$R = R_0 \left/ \left(1 - \frac{u_*}{q_0 \sqrt{K_I}}\right)\right., \quad (17b)$$

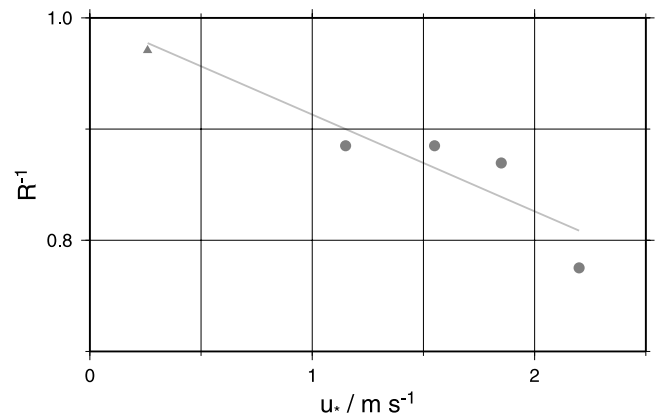


Figure 1. Inverse frictional parameter ($1/R$) as a function of u_* for the data sets presented in Table 1.

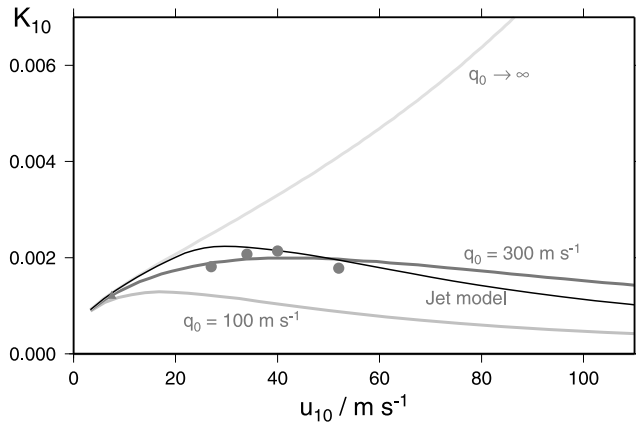


Figure 2. Drag coefficient (K_{10}) obtained from equation (8) as a function of u_{10} for $q_0 = 100 \text{ m s}^{-1}$, $q_0 = 300 \text{ m s}^{-1}$, and $q_0 \rightarrow \infty$ shown by shaded curves. The solid curve shows K_{10} computed from the jet ejection model for droplets (equation (49)).

where $R_0 = 1$, and $q_0 = 1/(a\sqrt{K_I})$ is a scale velocity, from which we have

$$K_R = K_I / (1 + u_1/q_0)^2 \quad (18a)$$

$$K_R = K_I \left[1 - u_* / (q_0 \sqrt{K_I}) \right]^2. \quad (18b)$$

At very large surface wind velocities, $K_R \rightarrow 0$, and

$$u_* = q_0 \sqrt{K_I}, \quad (19)$$

where q_0 is the sole velocity which determines u_* , and hence u_* tends to a constant. For $a = 0.087 \text{ m}^{-1}\text{s}$, we have $q_0 \sim 300 \text{ m s}^{-1}$. The key property of this frictional regime can be deduced by differentiating (8) with respect to u_* , which yields

$$-\frac{1}{2} K_{10}^{-3/2} dK_{10}/du_* = [1/\sqrt{K_I} - 2/(\kappa R)] dR/du_* - 2/(\kappa u_*). \quad (20)$$

[14] Equation (20) indicates that for a constant R , K_{10} increases monotonically with u_{10} . This is the traditional form for the drag coefficient relationship. For the linear dependence of R on u_1 , represented by (17a) (17b), however, we find from (20) that a maximum in drag coefficient with respect to u_* (or u_{10}) occurs for $R = R_m$, where

$$R_m = 1 + \frac{2\sqrt{K_I}}{\kappa}, \quad (21)$$

which indicates that the maximum drag coefficient occurs for an intrinsic drag coefficient (K_R) which is independent of the scale velocity (q_0), and on evaluating (21) we obtain

$R_m = 1.19$ ($r_m = -3.58$). Other properties at the maximum in K_{10} are the following:

friction velocity

$$(u_*)_m = q_0 \left[(2K_I/\kappa) / \left(1 + \frac{2\sqrt{K_I}}{\kappa} \right) \right]; \quad (22)$$

10-m velocity

$$(u_{10})_m = \frac{q_0 \sqrt{K_I}}{\kappa} \times \frac{2 - \ln[2K_I B^2 q_0^2 / (z_{10} g \kappa^2)]}{1 + \kappa / (2\sqrt{K_I})}; \quad (23)$$

10-m drag coefficient

$$(K_{10})_m = K_I \left\langle \frac{q_0}{\left\{ (u_{10})_m \left[1 + \kappa / (2\sqrt{K_I}) \right] \right\}} \right\rangle^2. \quad (24)$$

[15] The 10-m drag laws resulting from the application of (8) for a series of scale velocities (q_0) are illustrated in Figure 2. For $q_0 \rightarrow \infty$, the monotonic behavior of the growing wind wave sea occurs, whereas for $q_0 = 300 \text{ m s}^{-1}$ (which approximately represents the observations shown in Table 1) a maximum drag coefficient, $(K_{10})_m$, of 1.99×10^{-3} occurs at $(u_{10})_m = 42 \text{ m s}^{-1}$ with $(u_*)_m = 1.88 \text{ m s}^{-1}$. It is also apparent that the drag coefficient has a broad maximum with respect to u_{10} . For $q_0 = 100 \text{ m s}^{-1}$, the maximum occurs at a much lower wind speed, u_{10} , and the gradual approach to the high surface wind speed limit (19), which occurs for $u_* = 3.87 \text{ m s}^{-1}$, at which $K_{10} \rightarrow 0$ and $u_{10} \rightarrow \infty$, is clearly shown.

[16] The linear model thus reproduces both the position and shape of the maximum in the drag coefficient. The important question is what is its physical basis? From the point of view of the frictional regime, the constant q_0 model implies an atmospheric Ekman layer in which the similarity constant (C) decreases with u_{10} , giving rise to a frictional parameter (R) and an angle of turning (μ) which both increase, reaching respectively, $R = 1.3$ ($r = -2.7$, $C = 0.021$) and $\mu = 21^\circ$ for the highest wind speeds shown in Table 1, at which the intrinsic drag coefficient K_R has decreased to 8.9×10^{-4} . The physical mechanism represented by this evolution is the progressive formation of a “slip” surface at the sea surface. In section 4, we argue that this is due to spray production.

4. Spray Model

4.1. Nature of Spray

[17] The presence of spray at the sea surface indicates that the momentum imparted by the wind is partitioned between wave generation and spray production; see *Andreas* [2004]. The physical processes occurring in the growing wind wave sea, where the Stokes shear dominates over the Eulerian shear, makes no allowance for the existence of spray. The frictional loss occurring in the storm system, however, is fundamentally due to spray production, which is essentially the waste product of the wave generation mechanism.

[18] We will now interpret (17), as a spray model, assuming that the calibration, $q_0 = 300 \text{ m s}^{-1}$ is applicable. The consequences of this calibration for various aspects of the air-sea dynamics will be investigated.

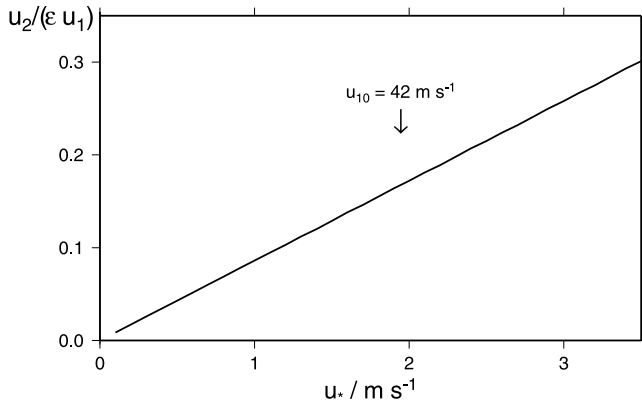


Figure 3. Ratio $u_2/(\epsilon u_1)$ as a function of u_* for $q_0 = 300 \text{ m s}^{-1}$.

4.2. Flattening of the Sea State

[19] A characteristic of the sea state in hurricane winds is that the waves appear to be flattened by the wind. This effect can be quantified using the spray model. We adopt the Toba wave spectrum for the growing wind wave sea, truncated at the peak wave number (k_0), for which

$$E = \frac{1}{3} \gamma_0 u_* c_0^3 / g^2, \quad (25)$$

where $E = \langle \zeta^2 \rangle$ is the root mean square wave height, and γ_0 is Toba's constant. On substituting for u_* , we obtain

$$E = \frac{1}{3} \gamma \sqrt{K_I} c_0^4 / (g^2 B), \quad (26)$$

where $\gamma = \gamma_0/R$. Hence the reduction in wave energy, due to spray, can be interpreted in terms of a reduced Toba constant (γ). In the limit of large surface wind velocities, $\gamma \rightarrow 0$, indicating a totally flattened sea state, and at $(K_{10})_m$, $\gamma/\gamma_0 = 0.84$, indicating a mild flattening in which the wave height is reduced by about 8%. The peak wave speed, $c_0 \rightarrow \infty$ for large surface wind velocities, and at $(K_{10})_m$, c_0 increases by about 20% because of the spray effect. Thus the production of spray tends to increase the wave speed of the peak wave, i.e., to transfer energy to longer wavelengths. The level of predicted flattening is in general agreement with that obtained by independent reasoning by *Jenkins* [2002].

4.3. The Similarity Profile at Extreme Wind Speeds

[20] The key result of section 3 is that the drag coefficient passes through a maximum, $(K_{10})_m$, with wind speed, and then is almost constant over a wide range of higher speeds, see Figure 2. Hence for the purposes of hurricane dynamics, where $(K_{10})_m$ occurs at about 40 m s^{-1} , the drag coefficient is “capped” at its maximum value over the full range of extreme wind speeds that are likely to occur.

[21] The physical processes which bring about this apparent similarity regime for extreme wind speeds are a dilation of the wave boundary layer, in which its thickness (z_B) and nondimensional velocity scale (u_1/u_*) both increase, but without a significant change in K_{10} ; see (1). The dynamical process which is occurring, is that as the

friction velocity increases, there is a progressive increase in the return flow of momentum from the ocean to the atmosphere because of the oceanic (Eulerian) shear in comparison with that from the atmosphere to the ocean because of the atmospheric shear. This two-way momentum exchange across the air-sea interface is represented by the two terms on the right-hand side of (2), the first of which arises from the atmospheric shear, and the second from the oceanic shear. Using (3) and (4), the ratio of the two shears,

$$u_2/(\epsilon u_1) = -1/(2r + 1). \quad (27)$$

[22] For the growing wind wave sea, $u_2/(\epsilon u_1) = 0$, whereas with the inclusion of spray production, $u_2/(\epsilon u_1)$ increases with u_* , and at $r = r_m$, $u_2/(\epsilon u_1) = 0.16$ (Figure 3). The increase over the range in u_{10} from about 30 to 60 m s^{-1} gives rise to an almost constant K_{10} over this range through corresponding changes in z_B and u_1/u_* .

4.4. Spray Velocity

[23] We look now at the energetics of spray formation, making use of the following expression for the rate of working on the wave field:

$$W = \rho_1 u_*^2 u_L, \quad (28)$$

where u_L is the velocity at which the transfer of momentum to the wave field is centered [*Bye and Wolff*, 2001]. On substituting for u_L , using (3) and (4), we obtain

$$W = \frac{1}{2} \rho_1 u_*^3 (2R - 1) / \sqrt{K_I}. \quad (29)$$

The rate of working (W) can be usefully partitioned into the two components,

$$W = W_0 + W_S, \quad (30)$$

where $W_0 = \frac{1}{2} \rho_1 u_*^3 / \sqrt{K_I}$ is the rate of working on the growing wind wave field, and

$$W_S = \rho_1 u_*^2 p \quad (31)$$

is the rate of working which generates the spray, where

$$p = u_* (R - 1) / \sqrt{K_I} \quad (32)$$

is the spray velocity. At the maximum of the 10-m drag coefficient, $(K_{10})_m$,

$$(W_S/W_0)_m = \frac{4\sqrt{K_I}}{\kappa}, \quad (33)$$

and the spray velocity, $(p)_m = 2(u_*)_m/\kappa$. Hence, on evaluating (33), we find that just over one quarter of the rate of working is used for spray production, and three quarters are used for wave growth [$(W_S/W_0)_m = 0.39$]. This partitioning of the rate of working highlights that the changes occurring in the wave field, described in section 4.2,

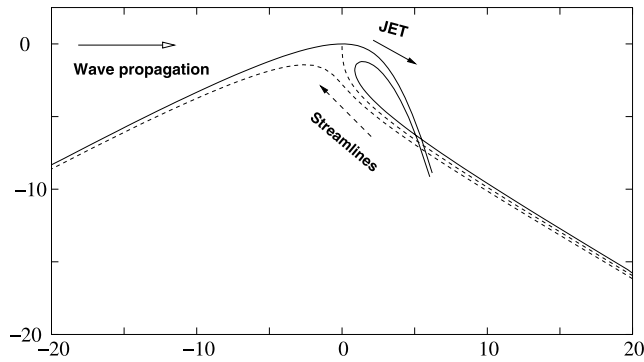


Figure 4. Ejection of fluid from a breaking-wave crest [after Jenkins, 1994]. The major axis of the overturning loop is approximately $8g^{-1/3}\Psi^{2/3}$, where Ψ is the flux of fluid in the jet. The vertical and horizontal axes are labeled in terms of the length scale $g^{-1/3}\Psi^{2/3}$. The relative speed of the fluid in the jet and the main body of water at the “impact point” is $6.9(g\Psi)^{1/3}$. Figure © Cambridge University Press 1994, reprinted with permission.

are due to spray production. For $q_0 = 300 \text{ m s}^{-1}$, the spray velocity, $(p)_m = 9.4 \text{ m s}^{-1}$, and for $W_0 = W_s$, the friction velocity (u_*) is 3.9 m s^{-1} , which is very similar to that of 4.2 m s^{-1} , predicted by *Andreas and Emanuel* [2001] for the condition that the spray stress and the interfacial stress are equal, strongly supporting the choice of $q_0 = 300 \text{ m s}^{-1}$ in the spray model.

4.5. Property Transfer Across the Sea Surface

[24] The implications of the partitioning of the rate of working into a wave (W_0) and a spray (W_s) component are apposite. The wave component (W_0) has no significance for property transfers across the sea surface; these are encompassed by the spray component (W_s). In the event that processes other than spray production are unimportant at extreme wind speeds, as proposed by *Emanuel* [2003], heat and momentum transfer should be governed by the same physics. Thus, on expressing the surface shear stress ($\tau_S = \rho_1 u_*^2$) in terms of the spray velocity, we have

$$\tau_S = \rho_1 C_S p^2, \quad (34)$$

where C_S is a drag coefficient appropriate to the spray production, and the net upward heat flux is

$$F = \rho_1 C_p C_S p (T_S - T_W), \quad (35)$$

where the drag coefficients (C_S) in (34) and (35) are identical, T_S is the surface water temperature, T_W is the wet bulb temperature of the descending spray particles, and C_p is the specific heat of water at constant pressure [*Emanuel*, 2003]. Equation (35) is of the same form as that applicable for heat exchange due to rainfall, in which p is replaced by the precipitation velocity (P) [see, e.g., *Bye*, 1996], except that, while P is a vertical velocity, p is a horizontal velocity. Allowance for evaporative heat exchange can also be made, and it is found that the drag coefficient for enthalpy transfer

at the temperatures occurring in hurricanes is similar to that for heat [*Emanuel*, 2003].

[25] In summary, at extreme wind speeds in which property transfers across the sea surface are dominated by spray production, the drag coefficients (C_S) for momentum and heat transfer, relative to the spray velocity (p), and hence also the drag coefficients (K_{10}) relative to u_{10} , are identical, and since the momentum drag coefficient (K_{10}) is “capped,” as discussed in section 4.3, that for heat transfer is also capped.

4.6. Volume Flux, Vertical Distribution of Spray Droplets, and Effect on Mean Flow Profile

[26] In the above analysis, the spray dynamics are represented through two processes: (1) the horizontal velocity (32) of the spray particles at formation and (2) the roughness relation (12), which modifies the wind profile because of the presence of the spray particles. It is instructive to consider these two processes using a physically based model.

4.6.1. Spray Production

[27] For a wind-sea state given by (25), we may assume that the momentum flux $\rho_1 u_*^2$ from the atmosphere acts to increase the wave momentum, and that the greater part of the wave momentum thereby generated is dissipated more or less immediately by wave breaking. The breaking of surface waves, though it is a complicated, time-dependent process, is, when sufficiently vigorous, usually characterized by the ejection of water in a forward directed jet at the crest. One of the simpler parameterizations of wave breaking which reproduces this feature is the stationary potential-flow model of *Jenkins* [1994], in which the jet is attached to a modified Stokes 120° corner flow, and where there is a unique relation between the geometrical length scale of the breaking structure and the flux of fluid in the jet (see Figure 4). In the frame of reference moving with the wave crest, the jet impacts the forward surface of the wave with a velocity, v_J , which depends on the size of the breaking-crest structure, and which in practice will be a fraction of the wave phase speed c . On contact with the forward face of the wave, the dissipation of the kinetic energy may go toward reducing the wave energy, but may also contribute to increasing the surface interfacial energy by the formation of droplets [*Andreas*, 2002].

[28] In this process, a proportion (β_J) of the surface shear stress ($\rho_1 u_*^2$) would be used in spray generation, and give rise to a mass flux per unit area,

$$G = \beta_J \rho_1 u_*^2 / v_J, \quad (36)$$

where, on comparing with the relations in section 4.4,

$$\beta_J = W_s / W \quad (37)$$

$$p = \beta_J v_J. \quad (38)$$

4.6.2. Spray Vertical Distribution

[29] To estimate the vertical distribution of spray droplets, we assume that they diffuse randomly with a (turbulent) diffusion coefficient $\sim \kappa u_* z$, but descend under gravity at a

terminal velocity w_t . To determine the terminal velocity, we need to specify a typical droplet radius r_s : in fact, a typical radius for the largest droplets, since the mass of a droplet is proportional to the cube of its radius. We assume that r_s is determined by a balance between the airflow tending to tear the droplet apart (represented by $\rho_1 u_1^2 = \rho_1 u_*^2 / K_I$) and the forces of surface tension (T) holding it together. By dimensional analysis, we have

$$r_s \sim \alpha_r T K_I / (\rho_1 u_*^2), \quad (39)$$

where α_r is a constant. To compute w_t we note that a typical value for r_s would be $87.5 \mu\text{m}$ (for $\alpha_r = 1.0$, $T \sim 70 \times 10^{-3} \text{ N m}^{-1}$, $K_I \sim 1.5 \times 10^{-3}$, $\rho_1 \sim 1.2 \text{ kg m}^{-3}$, and $u_* \sim 1 \text{ m s}^{-1}$), and droplets of this radius fall in the atmosphere in a regime intermediate between Stokes flow and fully turbulent flow [e.g., *Beard*, 1976]. Beard derived a relatively complicated expression for the dependence of w_t on r_s , but this may be simplified by inspection of his Figure 6, which gives the following approximate relation:

$$w_t \sim f_s r_s, \quad (40)$$

with $f_s = 8 \times 10^3 \text{ s}^{-1}$, for droplets of radius between approximately 0.01 mm and 1 mm . The terminal velocity for larger droplets increases more slowly with increasing radius, as a result of the droplet shape becoming flattened, and tends to a constant value of approximately 9 m s^{-1} for the largest droplets.

[30] If spray droplets suspended in the air contain a mass ρ_s of water per unit volume, in a steady state with no net vertical spray flux we will have

$$\kappa u_* z (d\rho_s/dz) + w_t \rho_s = 0. \quad (41)$$

Solutions to this equation are of the form

$$(\rho_s/\rho_{s0}) = (z/z_0)^{-w_t/(\kappa u_*)}, \quad (42)$$

where ρ_{s0} is the ‘‘surface’’ value of ρ_s , which, from (36), must satisfy, under steady state conditions,

$$w_t \rho_{s0} = \beta_J \rho_1 u_*^2 / \nu_J. \quad (43)$$

[31] It should, however, be noted that the integral of the solution in (42) diverges as $z \rightarrow \infty$ if $u_* \geq (u_*)_c$, where $(u_*)_c = w_t/\kappa$, so a steady state vertical distribution of spray droplets will not be attainable in this case. On evaluating, we obtain, $(u_*)_c = 1.2 \text{ m s}^{-1}$, which interestingly is similar to the friction velocity likely to be encountered in very high winds, see Table 1, and consistent with the anecdotal statement that ‘‘in hurricane conditions, the air is too thick to breathe and the water is too thin to swim in’’ [*Kraus and Businger*, 1994, p. 58]. Nevertheless, we assume that the droplets do become distributed according to (42) in a sufficiently deep layer for our purposes. This response arises from the classical form of the diffusivity,

$D = \kappa u_* z$, used in (41). For a constant D , the solution of (41) is

$$\rho_s/\rho_{s0} = \exp(-w_t z/D),$$

the integral of which converges unconditionally for all D . This model was used by *Lighthill* [1999] in an elegant study of the spray distribution brought about by wind gusts, in which he showed that $D = (1/6) Z^2/T$, where T is the ‘‘time of flight’’ for the coherent vertical displacement of a small particle of air because of a random gust which gives it a vertical displacement of equal probability over the range $-Z$ to $+Z$.

4.6.3. Effect of Suspended Spray Droplets on the Mean Flow Profile

[32] The dynamical effect of spray droplets has been estimated by *Makin* [2005], using the theory of *Barenblatt* [1953, 1979] for the effect of suspended particles in a turbulent flow. Barenblatt’s theory applies only in the case where $u_* \geq (u_*)_c$, and the predicted effect of the droplet suspension on the mean flow depends only on the terminal velocity and not on the droplet concentration. In this section we employ a different theory: a modification of the Monin-Obukhov theory for stratified boundary layers. We assume that

$$(\kappa z/u_*) (du/dz) = \phi_1(z/L), \quad (44)$$

where the Monin-Obukhov length L is given by

$$L = -u_*^3 \rho_1 / (\kappa g \Phi_b) = u_*^3 \rho_1 / (\kappa g w_t \rho_s), \quad (45)$$

where Φ_b is the vertical turbulent buoyancy flux, in the steady state equal to $-w_t \rho_s$, and the universal function $\phi_1(z/L)$ is, according to *Businger et al.* [1971]:

$$\phi_1(z/L) = 1 + 6z/L, \quad \text{for } 0 < z < L. \quad (46)$$

[33] The value of $\phi_1(z/L)$ for $z > L$ from experimental measurements appears to be rather uncertain, but in the calculations we present below, L is always much greater than the reference height of 10 m .

[34] From (42)–(45) we obtain

$$L = [u_* \nu_J / (g \kappa \beta_J)] (z/z_0)^{w_t/(\kappa u_*)} \quad (47)$$

$$\begin{aligned} du/dz &= [u_*/(\kappa z)] + 6g(\beta_J/\nu_J)(z/z_0)^{-w_t/(\kappa u_*)}, \\ &0 < z < L. \end{aligned} \quad (48)$$

[35] Now the boundary condition at the surface ($z = z_0$) should not be $u = 0$, but $u = (\rho_{s0}/\rho_1)\nu_J$, to account for the spray being injected horizontally into the water column [*Kudryavtsev*, 2005, also Effect of sea drops on atmospheric boundary layer at high wind conditions, preprint, 2005]. Integrating upward from $z = z_0$, we obtain

$$\begin{aligned} u &= (u_*/\kappa) \ln(z/z_0) + (\rho_{s0}/\rho_1)\nu_J + 6g(\beta_J/\nu_J) \\ &\times \{1 - [w_t/(\kappa u_*)]\}^{-1} z_0 \left[(z/z_0)^{1-w_t/(\kappa u_*)} - 1 \right]. \end{aligned} \quad (49)$$

[36] Equation (49) suggests that if $u_* \leq (u_*)_c$, the effect of the spray formation on the velocity profile is very small: However, for $u_* \geq (u_*)_c$ it becomes significant. The black curve in Figure 2 shows the value of the 10-m drag coefficient, $K_{10} = (u_*/u_{10})^2$, computed from (49), with the following parameters: $\kappa = 0.4$, $\beta_J = 0.15$ (which was estimated from (37) for $R \approx 1.1$), $\alpha = 0.018$, $T = 70 \times 10^{-3} \text{ N m}^{-1}$, $\rho_1 = 1.2 \text{ kg m}^{-3}$, $\rho_2 = 1000 \text{ kg m}^{-3}$, $\alpha_r = 1.0$, and $v_J = 0.5u_*/(\sqrt{K_I})$, which follows directly from (38). Note that the departure from the growing wind wave sea relation ($q_0 \rightarrow \infty$) becomes significant for $u_{10} \geq 22 \text{ m s}^{-1}$ ($u_* \geq 1.2 \text{ m s}^{-1}$). We see that there are still some discrepancies between the value of the drag coefficient computed by this method and by (8): notably that the reduction in drag coefficient begins at a higher wind speed. The reason for this effect may be that we have assumed that the droplets have only one radius, and that this radius decreases relatively rapidly with increasing wind stress ($r_s \propto u_*^{-2}$). In reality, the droplets have a complex size distribution [Andreas, 2002, 2004], which may, by modifying the vertical distribution of droplet mass in (42), tend to reduce the negative slope of the drag coefficient curve in Figure 2.

5. Conclusion

[37] We have presented a unified boundary layer model for predicting the drag coefficient (K_{10}) for momentum exchange at the sea surface, which takes account of wave growth and also spray production. It is found that K_{10} passes through a broad maximum primarily because of the return flow of momentum from the ocean to the atmosphere, which increases with friction velocity (u_*). The physical processes, which become evident in this extreme wind speed “similarity range” are the flattening of the sea surface with the transfer of energy to longer wavelengths, together with the production of spray. On the assumption that heat transfer across the sea surface at extreme wind speeds is mainly due to spray production [Emanuel, 2003], it is argued that the drag coefficient for heat should be similar to that for momentum, and also “capped” at extreme wind speeds.

[38] The analysis uses a simple expression (17) to model spray production, which has the effect that the sea surface becomes asymptotically flat for wind speeds well beyond those expected in nature. Equation (17) is essentially a linear expansion about the classical growing wind wave state, which takes account of spray production, and is appropriate for an open ocean environment. We also consider in section 4.6 a physically based model for the drag reduction, with explicit assumptions for the spray droplet size and the horizontal velocity of injection of spray droplets into the air column [Kudryavtsev, 2005, also Effect of sea drops on atmospheric boundary layer at high wind conditions, preprint, 2005], which, when calibrated using the parameters of the inertially coupled boundary layer model, gives the same qualitative behavior for the wind velocity dependence of the drag coefficient. An especially interesting finding is that the classical expression for diffusivity in (41) suggests that a critical friction velocity, $(u_*)_c$ is applicable for droplets of a specified terminal velocity, above which their effect on the dynamics (and thermody-

namics) of the planetary boundary layer becomes very significant.

[39] The analysis suggests that the growing wind wave sea can be regarded as an open-ended sea state, which evolves into a mature sea state of intensity set by the synoptic situation, and with frictional properties determined by the atmospheric Ekman layer, through the similarity constant C (and hence r).

[40] A similar expansion to (17) can be made about the wave state applicable in wave tanks by a suitable choice of R_0 and q_0 . An analysis of the laboratory experiments at high wind speeds, however, is beyond the scope of this paper.

[41] **Acknowledgments.** This work was begun while J.A.T.B. was a Visiting Fellow at the Bjerknes Centre for Climate Research in September 2003 and was completed during a Fellowship at the Hanse Institute for Advanced Study in Delmenhorst, Germany, in July and August 2004. A.D.J. is supported by the Research Council of Norway under Project 155923/700. This is Publication A 115 of the Bjerknes Centre for Climate Research. Helpful comments by the Editor and two referees are gratefully acknowledged.

References

- Andreas, E. L. (2002), A review of the sea spray generation function for the open ocean, in *Atmosphere-Ocean Interactions*, vol. 1, edited by W. Perrie, pp. 1–46, WIT Press, Southampton, U. K.
- Andreas, E. L. (2004), Spray stress revisited, *J. Phys. Oceanogr.*, *34*, 1429–1440.
- Andreas, E. L., and K. A. Emanuel (2001), Effects of sea spray on tropical cyclone intensity, *J. Atmos. Sci.*, *58*, 3741–3751.
- Barenblatt, G. I. (1953), On the motion of suspended particles in a turbulent flow, *Prikl. Mat. Mekh.*, *17*, 261–274.
- Barenblatt, G. I. (1979), *Similarity, Self-Similarity, and Intermediate Asymptotics*, 218 pp., Springer, New York.
- Beard, K. V. (1976), Terminal velocity and shape of clouds and precipitation drops aloft, *J. Atmos. Sci.*, *33*, 851–864.
- Businger, J. A., J. C. Wyngaard, Y. Izumi, and E. F. Bradley (1971), Flux-profile relationships in the atmospheric surface layer, *J. Atmos. Sci.*, *28*, 181–189.
- Bye, J. A. T. (1988), The coupling of wave drift and wind velocity profiles, *J. Mar. Res.*, *46*, 457–472.
- Bye, J. A. T. (1995), Inertial coupling of fluids with large density contrast, *Phys. Lett. A*, *202*, 222–224.
- Bye, J. A. T. (1996), Coupling ocean-atmosphere models, *Earth Sci. Rev.*, *40*, 149–162.
- Bye, J. A. T. (2002), Inertially coupled Ekman layers, *Dyn. Atmos. Oceans*, *35*, 27–39.
- Bye, J. A. T., and J.-O. Wolff (2001), Momentum transfer at the ocean-atmosphere interface: The wave basis for the inertial coupling approach, *Ocean Dyn.*, *52*, 51–57.
- Bye, J. A. T., and J.-O. Wolff (2004), Prediction of the drag law for air-sea momentum exchange, *Ocean Dyn.*, *54*, 577–580.
- Bye, J. A. T., V. K. Makin, A. D. Jenkins, and N. E. Huang (2001), Coupling mechanisms, in *Wind Stress Over the Ocean*, edited by I. S. F. Jones and Y. Toba, pp. 142–154, Cambridge Univ. Press, New York.
- Charnock, H. (1955), Wind stress on a water surface, *Q. J. R. Meteorol. Soc.*, *81*, 639–640.
- Emanuel, K. (2003), A similarity hypothesis for air-sea exchange at extreme wind speeds, *J. Atmos. Sci.*, *60*, 1420–1428.
- Garratt, J. R., and G. D. Hess (2003), Neutrally stratified boundary layer, in *Encyclopedia of Atmospheric Sciences*, edited by J. R. Holton, J. A. Curry, and J. A. Pyle, pp. 262–271, Elsevier, New York.
- Jenkins, A. D. (1989), The use of a wave prediction model for driving a near-surface current model, *Dtsch. Hydrogr. Z.*, *42*, 133–149.
- Jenkins, A. D. (1992), A quasi-linear eddy-viscosity model for the flux of energy and momentum to wind waves, using conservation-law equations in a curvilinear coordinate system, *J. Phys. Oceanogr.*, *22*, 843–858.
- Jenkins, A. D. (1994), A stationary potential-flow approximation for a breaking-wave crest, *J. Fluid Mech.*, *280*, 335–347.
- Jenkins, A. D. (2002), Do strong winds blow waves flat?, in *Ocean Wave Measurement and Analysis: Proceedings of the Fourth International Symposium, WAVES 2001: September 2–6, 2001, San Francisco, Cali-*

- formia*, edited by B. L. Edge and J. M. Hemsley, pp. 494–500, Am. Soc. of Civ. Eng., Reston, Va.
- Kraus, E. B., and J. A. Businger (1994), *Atmosphere-Ocean Interaction*, 362 pp., Oxford Univ. Press, New York.
- Kudryavtsev, V. N. (2005), On the marine atmospheric boundary layer at very strong winds, paper presented at General Assembly, Eur. Geosci. Union, Vienna, Austria, 24–29 April.
- Lighthill, J. (1999), Ocean spray and the thermodynamics of tropical cyclones, *J. Eng. Math.*, 35, 11–42.
- Makin, V. K. (2005), A note on the drag of the sea surface at hurricane winds, *Boundary Layer Meteorol.*, 115, 169–176.
- Nicholls, S. (1985), Aircraft observations of the Ekman layer during the Joint Air-Sea Interaction Experiment, *Q. J. R. Meteorol. Soc.*, 111, 391–426.
- Powell, M. D., P. J. Vickery, and T. A. Reinhold (2003), Reduced drag coefficient for high wind speeds in tropical cyclones, *Nature*, 422, 279–283.
- Toba, Y. (1973), Local balance in the air-sea boundary process III. On the spectrum of wind waves, *J. Oceanogr. Soc. Jpn.*, 29, 209–220.
- Wu, J. (1980), Wind-stress coefficients over sea surface near neutral conditions—A revisit, *J. Phys. Oceanogr.*, 10, 727–740.
-
- J. A. T. Bye, School of Earth Sciences, University of Melbourne, Melbourne, Victoria 3010, Australia. (jbye@unimelb.edu.au)
- A. D. Jenkins, Bjerknes Centre for Climate Research, Geophysical Institute, Allégaten 70, N-5007 Bergen, Norway. (alastair.jenkins@bjerknes.uib.no)